Earth Planet. Sci. Lett. 677 (2026) 119812

Contents lists available at ScienceDirect

Earth and Planetary Science Letters

journal homepage: www.elsevier.com/locate/epsl

Ancient, buoyant mantle under the Sierra Leone Ridge in the equatorial Atlantic

Camilla Sani [a,b], Alessio Sanfilippo [b,*], Felix Genske [a], Carlotta Ferrando [c], Daniele Brunelli [e], Anna Cipriani [e], Alexander Peyve [d], Sergey Skolotnev [d], Marco Ligi [f], Andreas Stracke [a]

[a] Institut für Mineralogie, Universität Münster, Corrensstraße 24, D-48149 Münster, Germany
[b] Dipartimento di Scienze della Terra e dell'Ambiente, Università di Pavia, via Ferrata 1a, 27100 Pavia Italy
[c] Department of Earth, Environmental and Life Sciences, University of Genova, 16132 Genova, Italy
[d] Geological Institute, Russian Academy of Science, Pyzhevsky Lane 7, 119017 Moscow, Russia
[e] Dipartimento di Scienze Chimiche e Geologiche, Università di Modena e Reggio Emilia, Modena, Italy
[f] Istituto di Scienze Marine, Consiglio Nazionale delle Ricerche, via Gobetti 101, 40129 Bologna, Italy

ARTICLE INFO

Editor: Dr R. Hickey-Vargas.

Keywords:
MAR
MORB
Abyssal peridotites
Radiogenic isotopes
Mantle buoyancy

ABSTRACT

The Sierra Leone Ridge is the equatorial portion of the Mid-Atlantic Ridge (MAR) between the St. Paul (0–1°N) and Doldrums (7–9°N) Fracture Zones. At ~80 Ma, a submarine plateau –the Sierra Leone Rise which is now located off-ridge on the African plate and the Céarà Rise on the South American plate– formed due to excess magma production. Incompatible element-enriched MORB with high Sr-Pb but low Nd isotope ratios suggests that the high magma production could result from the interaction of a mantle plume with the Sierra Leone Ridge, the so-called Sierra Leone mantle plume that may now be centered at ~1.7°N along the MAR. In order to define the nature of the mantle source beneath the Sierra Leone Ridge, we present major-trace element concentrations and radiogenic isotope ratios from abyssal peridotites and MORB from 4 to 7°N along the MAR. High Hf isotope ratios are preserved in clinopyroxenes from abyssal peridotites ($\varepsilon_{Hf} = 12–54$), indicating that the mantle beneath the Sierra Leone Ridge underwent extensive melting several 10^8–10^9 years before remelting under the present MAR. Most peridotites have high ε_{Hf}, but low ε_{Nd} similar to MORBs, although some extend to unusually low ε_{Nd} of ~-6. We argue that these peridotites not only melted, but were also re-enriched in compatible elements concurrent to melting in the past, and that such incompatible element re-enriched peridotites are now the main component of the sub-ridge mantle in the Sierra Leone area. Extensive remelting of ancient, incompatible element re-enriched peridotite that is compositionally buoyant, in addition to minor amounts of recycled crust, may therefore have caused the abundant magmatism that characterizes this portion of the MAR since formation of the Sierra Leone and Céarà Rise ~80 Ma ago, and accounts for its elevated topography.

1. Introduction

Mantle melting at mid ocean ridges creates a range of peridotites from which different extents of melt have been extracted, and are thus variably depleted in incompatible elements. These melt-depleted peridotites have variably high Lu/Hf and Sm/Nd and, with time, develop Hf and Nd isotope ratios by far higher than those observed in mid-ocean ridge basalts (MORB) (e.g., Stracke et al., 2011; Stracke, 2021; Willig et al., 2020; Stracke and Salters, 2025). Such melt-depleted peridotites have been found at the Equatorial (Sani et al., 2023; Ferrando et al., 2024) and Northern Mid-Atlantic Ridge (MAR, Sanfilippo et al., 2024), at Gakkel Ridge (Stracke et al., 2011; Stracke and Salters, 2025), and the Southwest Indian Ridge (Woelki et al., 2025), in peridotite massifs, and within ophiolites (e.g. Guarnieri et al., 2012; Sanfilippo et al., 2019; Tilhac et al., 2022). Ancient melt-depletion not only leads to high Hf isotope ratios in peridotites today, but has also made them less dense (e.g. Schutt and Lesher, 2006; Afonso and Schutt, 2012; Stracke and Béguelin, 2024). The excess buoyancy of variably melt-depleted peridotites may influence ridge depth (Zhou and Dick, 2013; Woelki et al., 2025), but may also temporarily increase mantle flux through sub-ridge

* Corresponding author.
E-mail address: alessio.sanfilippo@unipv.it (A. Sanfilippo).

https://doi.org/10.1016/j.epsl.2025.119812
Received 29 April 2025; Received in revised form 20 December 2025; Accepted 25 December 2025
Available online 31 December 2025

melting regions and thus result in periods of excess melt production, without large temperature variations of the upwelling mantle (e.g., Morrow and Mittelstaedt, 2021; Sanfilippo et al., 2024; Béguelin et al., 2025).

Here, we present another case where the abundance of ancient, melt-depleted peridotites explains the shallow bathymetry and the high melt production along the equatorial Mid Atlantic Ridge (MAR), which has so far been related to the interaction with a hot mantle plume. We report new geochemical and radiogenic isotope ratios of abyssal peridotites and associated basalts from the equatorial MAR between ~4 – 7°N, the so-called Sierra Leone Ridge (Fig. 1). Previous studies suggested that the off-ridge Sierra Leone Rise may have formed by excess melting caused by a near-ridge mantle plume starting 80 Ma (Schilling et al., 1994). Consistent with upwelling and melting of hot, incompatible -element-enriched mantle under this section of the MAR, the MORB around 1.7°N –the present-day location of the postulated Sierra Leone hotspot– are enriched in incompatible and volatile (i.e., H_2O, F, and Cl) elements, and have comparatively high Sr–Pb, but low Nd isotope ratios (Schilling et al., 1994; Kelley et al., 2013; Le Voyer et al., 2015) (Fig. 2). From the isotope data of basalts and peridotites reported here, however, we infer that the sub-ridge mantle along the Sierra Leone Ridge is dominated by ancient, melt-depleted, but incompatible element re-enriched peridotites (Fig. 2). The abundant magmatism in this portion of the MAR may therefore have been initiated by upwelling of variably melt-depleted, buoyant, and chemically heterogeneous mantle since ~80 Ma. This may account for the high magma production rates without the need for upwelling of unusually hot mantle, i.e., a near-ridge thermal plume.

2. Geological setting and sample selection

The study area is located in the northern portion of the Equatorial MAR between the Doldrums Fracture Zone (FZ) in the north at ~8°N and the St. Paul FZ at ~1°N. The Strakhov FZ at 4°N offsets the MAR in this area by approximately 130 km to the east. The MAR shallows between ~ 1–7°N near the off-ridge Sierra Leone Rise. This section of the MAR has been termed Sierra Leone Ridge (Fig. 1).

The great depth of the equatorial MAR and the low degrees of mantle melting inferred for the MORB in this area may indicate a regional thermal minimum of the sub-ridge mantle (Bonatti et al., 1993). The shallow Sierra Leone Ridge, however, may be caused by higher magma production rates due to upwelling of a near-ridge plume, the Sierra Leone (SL) plume (Schilling et al., 1994). The activity of the postulated SL plume may have started ~80 Ma ago when abundant magmatism

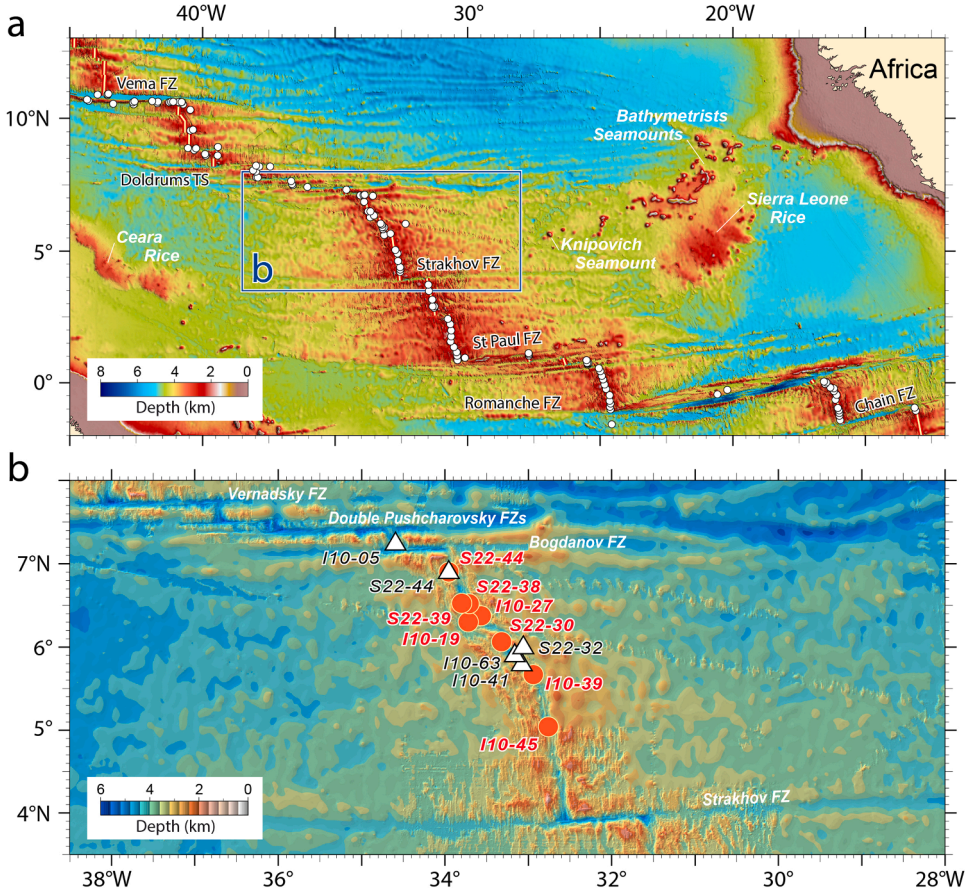

Fig. 1. Bathymetric maps of the Equatorial MAR. (a) Shaded relief image derived from a 200 m grid compilation of our multibeam data (Bonatti et al., 1994; Udintsev, 1996; Ligi et al., 2002, 2022; Skolotnev et al., 2003, 2020) and additional data from the NOAA National Centers for Environmental Information Multibeam Bathymetry Database (doi:10.7289/V56T0JNC), merged with the GEBCO 2024 global bathymetric grid (GEBCO Bathymetric Compilation Group,). Multibeam data were processed using the Kongsberg Neptune/Poseidon packages, and spatial analysis and mapping were carried out with the PLOTMAP software (Ligi and Bortoluzzi, 1989). The map is shown in Mercator projection at 0°N, referenced to WGS84, with illumination from the northwest. The Sierra Leone swell and the traces of the major equatorial transforms extending between South America and Africa are clearly visible. The labeled box indicate the portion of the Equatorial MAR shown in (b). Locations of basaltic glasses collected along the ridge axis, from the PetDb database (https://search.earthchem.org/), are indicated by white circles. (b) Bathymetry of the Sierra Leone Ridge, bounded to the south by the Strakhov transform fault (TF) and to the north by the Doldrums transform system (TS). The Doldrums TS comprises five transform faults, listed from north to south: Doldrums, Vernadsky, North Pushcharovsky, South Pushcharovsky, and Bogdanov. Map displayed in Mercator projection at 6°N (datum WGS84), with sun illumination from the northwest. Dredging stations from this study are shown as orange filled circles (basaltic glasses) and white filled triangles (peridotites).

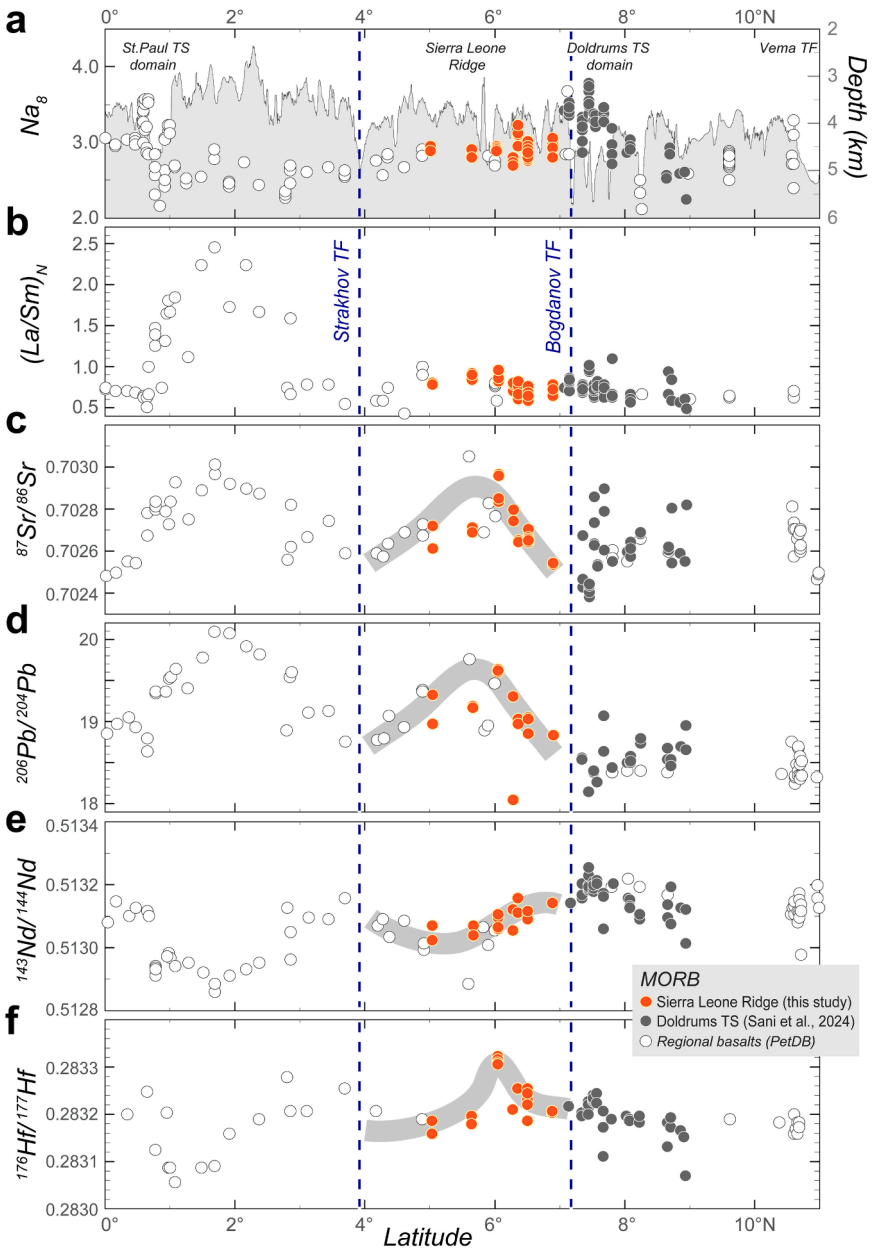

Fig. 2. Geochemical and isotopic variation of the erupted basalts from the Equatorial MAR. Along-axis latitudinal variations between 0° and 11°N of: (a) ridge-axis depth and Na_8 values; (b) primitive mantle–normalized $(La/Sm)_N$ ratios (McDonough and Sun, 1995); and (c–f) Sr, Pb, Nd, and Hf isotopic ratios of MORB. Major transform faults (TFs) separating distinct geochemical regions are shown as dashed blue lines. The thick gray pattern marks the geochemical trend defined by MORBs from this study (Sierra Leone Ridge basalts). Red filled circles: basalts from this study; dark gray filled circles: basalts from Sani et al. (2024); white filled circles: regional basalts from PetDB (www.earthchem.org/petdb).

formed a submarine plateau, which is now separated into the off-ridge Sierra Leone Rise on the African plate and the Céarà Rise on the South American plate (Fig. 1). After recent (<10 Ma) westward migration of the ridge, the alleged SL plume may now be located at ~1.7 °N and ~ 30°W.

According to kinematic plate reconstruction models of the hot spot track that relate the Bathymetrists Seamount Province to the Sierra Leone plume activity (Basile at al., 2020), however, the current position of the SL plume would be ca. 100 km west of the 10 Ma-old recent Knipovitch Seamount at ~5°N (Fig. 1). On the other hand, based on different plate tectonic reconstructions (Sleep, 2002), and the available geochemical data, Long et al. (2020) considered a connection between the SL plume and the formation of the Bathymetrists Seamounts Province unlikely. But owing to the lack of samples from the Sierra Leone and Céarà Rises, it is difficult to establish a common geochemical affinity of basalts from these two plateaus with those from the Bathymetrist Seamounts Province and the MORB erupted along this section of the MAR.

3. Methods

In this study, we analyzed the major and trace element concentrations and the Sr-Nd-Hf-Pb isotope ratios of 39 basalt glasses, and the Nd-Hf isotope ratios of 9 abyssal peridotites recovered during two joint Russian-Italian oceanographic expeditions, the cruise n. 22° of the RV *Akademik Nikolaj Strakhov* (Peyve et al., 2003) and the cruise n. 10° of the RV *Akademik Ioffe* (Savel'eva et al., 2006). Basalts and fresh basalt glasses were recovered along the entire ridge section (Fig. 1). Peridotites were collected at the ridge-transform intersection within the

non-transform fault basin at 6.8°N, and the so-called *Markov Deep*, at ~6°N (Fig. 1).

3.1. Major element concentrations

Major element concentrations of clinopyroxenes and spinels of the abyssal peridotites, and whole rock analyses of basalt glasses were measured by electron probe microanalysis (EPMA) with a JEOL JXA 8200 Superprobe at the Department of Earth's Science Ardito Desio of Milano University. The analyses of all elements were performed with an accelerating potential of 15 kV, a beam current of 15nA, and a total 30-second counting time. All major element compositions are listed in Tables 1 and 2 in the Supplementary material.

3.2. Trace element concentrations

The trace element concentrations of clinopyroxenes and of the basaltic glasses were determined by laser ablation ICP-MS using a QQQ-ICP-MS Agilent Series 8900 interfaced to a GeoLas 193 nm excimer ablation system (Lambda Physik, Germany) at the CNR–IGG S.S. of Pavia. The ablation system was operated at a 10 Hz repetition rate, fluence of about 9 J/cm^2, and 50 μm spot size for the MORB glasses and 100 μm spot size for the cpx. Helium was used as carrier gas and mixed with Ar downstream of the ablation cell. The NIST SRM 610 synthetic glass was used as an external standard, with ^{44}Ca as internal standard for clinopyroxene analyses and ^{29}Si for the basaltic glasses. Background and signal intensities were measured for about 60 s; the raw data were reduced using the software package GLITTER® using the NIST SRM 610, and NIST SRM 612 as crosscalibration, with values of Jochum et al. (2011). Precision and accuracy were assessed by repeated analyses of the BCR-2 g, BIR 1 and BHVO 2 reference material and are better than ±10 %, with most elements below ±5 %. All trace element compositions and reference material are listed in tables S1, S2, S3 and S5 in the Supplementary material.

3.3. Sr-Nd-Hf-Pb isotope ratios measurements

The Nd and Hf isotope ratio measurements of clinopyroxene separated from the peridotites were performed at the Institut für Mineralogie, Universität Münster, following the same procedure as in Sani et al. (2023). The Sr-Nd-Hf-Pb isotope ratios of basalt glasses were processed following the procedure described in Sani et al. (2024). Both the clinopyroxene separates (~70–150 mg, hand-picked under binocular microscope) and the basalt glasses (~150 mg glass chips hand-picked under a binocular microscope) were leached with H_2O_2 and 6 N HCl to remove the effects of seawater alteration. The grains were dissolved in concentrated HF:HNO_3 (4:1). Strontium, the high field strength element (HFSE) and rare earth element (REE) fractions of the samples were separated on a standard cation exchange column (resin Biorad® AG50W-X8, mesh size 200–400 μm). Hafnium was purified from the HFSE fraction using Eichrom® Ln Spec columns (Münker et al., 2001). Neodymium was further purified from the REE fraction in a second column, using an Eichrom® Ln Spec resin (mesh size 50–100 μm). For the basaltic glasses, Pb was extracted and purified with HBr-HNO_3 following the protocol given in Todd et al. (2015) using an AG1-X8 100–200 μm mesh anion exchange resin (Lugmair and Galer, 1992). All samples were processed twice through the columns to improve the separation of Pb from the sample matrix. The Sr, Nd, Hf and Pb isotope ratios were determined on a Thermo Scientific NEPTUNE *Plus* MC-ICP-MS at Universität Münster. All Sr cuts were measured in 10 ppb solutions and were bracketed by reference material NBS987. All data were normalized to NBS987 ^{87}Sr/^{86}Sr = 0.710248. The USGS rock standards BHVO-2 and BCR-2 gave ^{87}Sr/^{86}Sr = 0.703495 ± 15 (2 S.E.) and ^{87}Sr/^{86}Sr = 0.705020 ± 6 (2 S.E.). For the Tl-doped Pb isotope analyses via MC-ICP-MS precision was determined by analyses of BCR-2 and BHVO-2. Lead isotope ratios of BCR-2 gave ^{206}Pb/^{204}Pb = 18.7718 ± 22 (2 S.E.), ^{207}Pb/^{204}Pb = 15.6374 ± 18 (2 S.E.), and ^{208}Pb/^{204}Pb = 38.7824 ± 47 (2 S.E.). Lead isotope measurements of BHVO-2 gave ^{206}Pb/^{204}Pb = 18.6730 ± 17 (2 S.E.), ^{207}Pb/^{204}Pb = 15.5668 ± 16 (2 S.E.), and ^{208}Pb/^{204}Pb = 38.3185 ± 42 (2 S.E.). Repeated measurements of the JMC-475 Hf standard gave an average ^{176}Hf/^{177}Hf = 0.282160 ± 13 (2 S.D., n = 8, 10–30 ppb solution). All Hf isotope ratios are reported relative to ^{176}Hf/^{177}Hf = 0.282160 (Blichert-Toft and Albar`ede, 1997; Münker et al., 2001). To verify accuracy of the Hf isotope ratio measurements, USGS rock reference materials BHVO-2 and BCR-2 were processed as unknowns and gave ^{176}Hf/^{177}Hf = 0.283096 ± 25 (2 S.D., n = 12) for BHVO-2 and ^{176}Hf/^{177}Hf = 0.282867 ± 20 (2 S.D., n = 10) for BCR-2. The JNdi-1 (20 ppb) Nd bracketing standard was determined at ^{143}Nd/^{144}Nd = 0.512067 ± 11 (2SD, n = 7), and all data are normalized to JNdi-1 ^{143}Nd/^{144}Nd = 0.512115. The USGS rock standard BHVO-2 gave ^{143}Nd/^{144}Nd = 0.512981 ± 18 (2 S.D., n = 8) and ^{143}Nd/^{144}Nd = 0.512641 ± 12 (2 S.D., n = 5) for BCR-2. Duplicate isotope measurements for samples S22–30–54, S22–30–59, S22–30–60, S22–30–68 reproduced within analytical uncertainty. All data are given in tables S1 and S4 in the Supplementary material.

4. Results

4.1. Mantle peridotites

Peridotite samples were characterized with optical microscopy, and their modal mineralogy was estimated by point counting. Serpentine with mesh texture and associated magnetite was attributed to olivine (Ol), whereas bastitic serpentine was attributed to orthopyroxenes (Opx). Selected peridotites range from harzburgites to Cpx-poor lherzolites. Based on the petrography and the clinopyroxene (Cpx) content we identified 3 lherzolites (> 5 % Cpx) and 6 harzburgites (< 5 % Cpx). In detail, peridotites from the ridge-transform intersection located at ~7.25 °N (**I10–5/5** and **I10–5/8**) are harzburgites with porphyroclastic texture and Opx occurring as coarse-grained and commonly deformed porphyroclasts, showing *kink bands* and undulose extinction. Clinopyroxene is fine grained and occurs mainly in association with neoblastic Opx and spinel or with anhedral habit, interstitial to olivine (Ol) and Opx. The sample from the 6.8°N non-transform fault (**S22–44/14)** is a harzburgite with ~3–4 vol. % Cpx with porphyroclastic texture and with Opx locally occurring as mm-size clusters. The rest of the peridotites are from the so-called Markov Deep at ~6°N (Fig. 1), a deep basin with a maximum depth of 5000 m. Peridotites from this location are generally less serpentinized and preserve fresh Ol in small relict crystals. The Opx are present as large deformed crystals with kink bands and have elongated habits. Spinel is present as medium-sized crystals with rims altered to magnetite. Samples **S22–32/1, S22–32/5** and **I10–41/19** are spinel harzburgites whereas sample **S22–32/2** is a lherzolite with equigranular texture, with up to 0.5 mm large Cpx, and rare fresh Ol cores. Lherzolites **10–63/36** and **I10–63/37** preserve large, deformed Cpx porphyroclasts up to 1 mm long and have abundant spinel interstitial to large Ol crystals. Two samples from Markov Deep (**S22–32/2** and **I10–41/19)** have trace contents of plagioclase, completely altered within submillimeter-sized veins between the peridotitic minerals, and commonly associated to Opx.

The mineral compositions of lherzolites and harzburgites do not show any substantial differences, and there is also no compositional difference between the peridotites from the different locations. Overall, all peridotites have spinel Cr# (Cr/(Cr+Al)) ranging between ~ 22 and 50 mol % whereas Mg# (Mg/(Mg+Fe)) ranges between 50 and 75 mol % (Fig. 1 in the supplementary material). The TiO_2 concentrations in Cpx are relatively low in all samples (0.2–0.1 wt. %), and decrease with increasing Cr# in coexisting spinels. Two samples deviate from the general trend, **I10–5/5** and sample **I10–41/19** with Cr# in spinel of 49 and 45 coupled with comparatively high TiO_2 in Cpx of 0.15 wt. %. The content in TiO_2 in spinel is < 0.1 wt. % in all samples, except for **I10–5/5**

and **I10–41/19** with 0.22 and 0.25 wt. % TiO_2, respectively. The Na_2O contents in Cpx of the studied peridotites range from ~0.1 to ~0.4 wt. %. Peridotites **I10–5/8, I10–63/37, S22–32/1/2/5** have Na_2O contents between 0.2 and 0.4 wt. %.

The majority of the abyssal peridotites from the Sierra Leone (SL) Ridge display variable REE patterns which differ in their light rare earth element (LREE) relative to middle rare earth element (MREE) and heavy rare earth element (HREE) contents, i.e., $(Ce/Sm)_N$ ranges from ~ 0.001 to 0.52 (Fig. 3). The absolute REE contents are also very variable, with Yb_N (subscript N indicating primitive mantle normalized, values by Mc Donough and Sun, 1995) ranging from 0.98 to 3.1. Four samples, **S22–32/1, S22–32/5, I10–5/5, I10–5/8** and **S22–44/14**, have high MREE and HREE contents (Yb_N of 2.4–3.15) in Cpx, nearly absent MREE/HREE fractionations ($(Gd/Yb)_N$ = 0.4–0.5), and moderate to strong depletion in LREE relative to MREE ($(Ce/Sm)_N$ = 0.003–0.036) (Fig. 3a). In contrast, **I10–63/36** and **I10–63/37** have enriched LREE ($(Ce/Sm)_N$ = 0.09–0.52), but low HREE contents (Yb_N = 0.98–1.11). **I10–41/19** and **S22–32/2** have flat REE patterns with high LREE contents ($(Ce/Sm)_N$ = 0.43–0.18) and subtle fractionation between MREE and HREE. Most peridotites have $^{176}Lu/^{177}Hf$ between 0.1 and 0.4 and $^{147}Sm/^{144}Nd$ from 0.3 to 1.4, with one sample (I10–63–37) having Cpx with $^{176}Lu/^{177}Hf = 1.8$.

The Nd-Hf isotope compositions of the SL Ridge peridotites are variable. Except for one sample with ε_{Hf} of 16 (**I10–41/19**), all samples have $\varepsilon_{Hf} > 25$, which is systematically higher than those of the local MORB (red circles in Fig. 4a). Despite ε_{Hf} between 16 and 54, the ε_{Nd} values range from −6 to +25, which is a greater range than basalts from the 0–10°N sector of the MAR, including the incompatible element enriched MORB from ~1.7°N (Fig. 4a). Two peridotites (**I10–63/36** and **S22–44/14**) with $\varepsilon_{Nd} < 0$ have ε_{Hf} of 31 and 47. Similarly, the sample with the highest ε_{Nd} (+25, **S22–32/5**) has ε_{Hf} of +51. Finally, TiO_2 and MREE-HREE contents of Cpx in the peridotites correlate positively with $^{143}Nd/^{144}Nd$ (Fig. 4b).

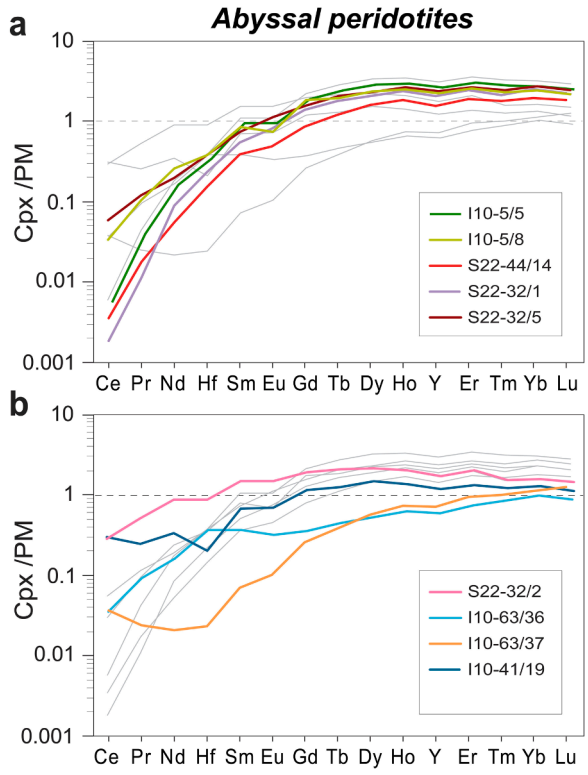

Fig. 3. Trace element compositions of clinopyroxene of the abyssal peridotites from the Sierra Leone Ridge. Primitive mantle–normalized REE patterns (McDonough and Sun, 1995). (a) Samples showing typical depleted mantle REE trends, characterized by LREE depletion and relatively flat HREE. (b) Samples showing anomalous REE patterns, with enrichments or irregularities in the middle to light REE range.

4.2. Basalts

Fresh glasses were recovered from the investigated on-axis basalts along the entire MAR segment between 5 and 7.6°N (Fig. 1). All basalt glasses are tholeiites, with SiO_2 between 46 wt. % and 52 wt. % and low alkali contents ($K_2O + Na_2O < 4.3$ wt. %), and similar CaO ~ 11 wt. %. At decreasing MgO contents, basalts show increasing TiO_2, Na_2O and K_2O, and decreasing Al_2O_3 due to synchronous Ol and Plagioclase (Plag) fractionation. Primitive mantle (McDonough and Sun, 1995) normalized trace element compositions have typical MORB like patterns with depletions in the most incompatible elements (Rb, Ba, Th, Nb and LREE) relative to the less incompatible elements (Sm, Eu, Gd, Ti and HREE) (Fig. 5a).

Basalts from the Sierra Leone (SL) Ridge have variable $^{143}Nd/^{144}Nd$ (0.5129–0.5131), $^{87}Sr/^{86}Sr$ (0.7023–0.7027) and $^{206}Pb/^{204}Pb$ (18.7–19.8), but $^{176}Hf/^{177}Hf$ distinctly higher (> 0.2833) compared to MORB from the area, 0–11°N along MAR (Figs. 2, and 5). In detail, the samples with high $^{87}Sr/^{86}Sr$ (up to 0.7029) and $^{206}Pb/^{204}Pb$ (up to19.7) also have the highest $^{176}Hf/^{177}Hf$ (up to 0.2833) among the samples collected from the area, but low $^{143}Nd/^{144}Nd$ (ca. 0.5130). These samples are also characterized by high $(La/Sm)_N$ of 0.8–0.9 and $(Nb/Zr)_N$ of ~0.7. The overall high Pb-Sr and low Nd isotope ratios of the Sierra Leone Ridge basalts are coupled with high large ion lithophile elements (LILE), LREE and Nb compared to basalts from the adjacent Doldrums area, which display higher Nd and lower Hf, Pb and Sr isotope ratios and depletion in the most incompatible trace elements (i.e., LILE, Nb, LREE).

Fig. 2 shows variations in ridge depth (km) and MORB chemistry for the entire 0–10°N MAR region as a function of latitude. Large-scale variations in ridge depth are mirrored by variations in Na_8 (Na_8 is the Na_2O content of basalts calculated at 8 wt. % MgO after Klein and Langmuir, 1987) and, to some extent, in Sr-Nd-Hf-Pb isotope ratios. At the St. Paul FZ, basalts from the intra-transform ridges have high Na_8 values (3–3.5) although they have relatively low Sr-Pb isotope ratios and relatively high Nd-Hf isotope ratios. Na_8 reaches the lowest values (Na_8 = 2.5) at ~1.7°N, which are associated with local increases in $(La/Sm)_N$, high Sr and Pb isotope ratios and low Nd-Hf isotope ratios, signatures that define the so-called 1.7°N anomaly (Schilling et al., 1994). At ~ 3°N the basalts have low La/Sm, and Sr-Pb isotope ratios associated with higher Hf-Nd isotope ratios. Between the Strakhov transform fault (TF) and Doldrums FZ further north, the studied samples (in orange) show a gradual increase of Na_8, Sr-Nd-Pb isotope ratios and $(La/Sm)_N$. At 6°N, high $^{206}Pb/^{204}Pb$ (~ 19.7) and $^{87}Sr/^{86}Sr$ (0.7029) basalts are associated with the highest $^{176}Hf/^{177}Hf$ (0.2833) of the entire ridge. From 6°N towards the Doldrums FZ domain, the Sr-Pb ratios decrease until reaching the lowest values of MORB from the entire 0–11°N segment (Sani et al., 2024). These signatures are coupled with an increase of Nd isotope ratios and moderately high Hf isotope ratios, Na_8, and $(La/Sm)_N$ (up to ~ 3.5 and 0.97, respectively, at the central ITRs of Doldrums). North of the Doldrums FZ, the geochemical and Sr-Nd-Hf-Pb isotope ratios are variable in the basalts.

5. Discussion

5.1. Nature of the Sierra Leone sub-ridge peridotites

Abyssal peridotites from the Sierra Leone (SL) Ridge have variable incompatible element contents, ranging from depleted to slightly enriched relative to bulk silicate Earth (e.g., McDonough and Sun, 1995). These variations are controlled by recent processes such as melt-depletion and/or re-enrichment by melt-rock reactions. Melt-depleted peridotites are characterized by low LREE to MREE ratios (e.g., $(Ce/Sm)_N = 0.08$ after 7 % of partial melting of a depleted mantle, DM, from Salters and Stracke (2004), Fig. 6 in the supplementary

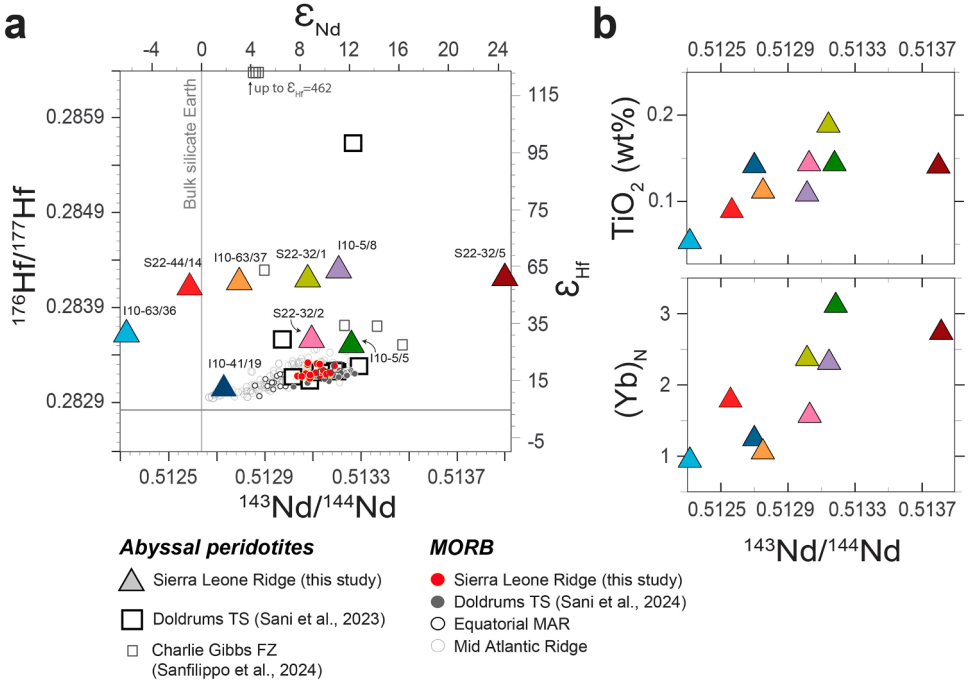

Fig. 4. Hf-Nd isotopic variations of the abyssal peridotites from Sierra Leone Ridge. (a) Diagram showing Hf and Nd isotope ratios of clinopyroxene (cpx) from Mid-Atlantic Ridge peridotites analyzed in this study (error bars smaller than the symbols). Abyssal peridotites from the Sierra Leone Ridge (this study), the Doldrums TS (Sani et al., 2023) and the Charlie Gibbs FZ (Sanfilippo et al., 2025) are shown as color-filled triangles (each color representing a different sample), empty black squares, and empty gray squared, respectively; circles represent MAR basalts (symbols and data sources as in Fig. 2). Note that clinopyroxenes from peridotites consistently display high Hf isotope ratios, locally associated with MORB-like, enriched, or depleted Nd isotope ratios. (b) Cpx TiO_2 and $(Yb)_N$ contents versus Nd isotope ratios of the peridotites. These plots show that abyssal peridotites, represented by color-filled triangles as in panel (a), with the lowest Yb and TiO_2 contents correspond to the lowest Nd isotope ratios, and vice versa.

materials), thus requiring post-melting processes to develop enrichments in incompatible elements, i.e., enrichments in LREE relative to MREE-HREE (Fig. 6). Such incompatible element re-enrichment may result from retaining or trapping small aliquots of LREE-enriched melt within the melt-depleted peridotites (e.g., Brunelli et al., 2006; Brunelli and Seyler, 2010; Seyler et al., 2007) and/or reaction with migrating melts (e.g., Godard et al., 1995; Warren et al., 2009; Sani et al., 2020). These "refertilization" processes mostly happen at the lithosphere-asthenosphere boundary, due to the sudden decrease in temperature that may enhance reactive crystallization of trapped or migrating melts (e.g. Niu, 2004; Brunelli and Seyler, 2010).

Most of the peridotite Cpx have incompatible trace element contents that cannot be explained by a partial melting event alone (Fig. 3a), for instance the LREE/MREE (i.e. $(Ce/Sm)_N$) in Cpx are higher than the residual compositions after partial melting as shown in Fig. 6. The REE patterns of the Cpx reflect only the final, integrated, stage of a multi-stage evolution of the peridotites by partial melting and "refertilization". However, most of the studied abyssal peridotites from the Sierra Leone Ridge have low TiO_2 in spinel (< 0.2 wt. %) and Na_2O in Cpx (< 0.4 wt. %), indicative of low extents of melt-rock reaction (e.g., Dick and Bullen, 1984; Hellebrand and Snow, 2003; Seyler et al., 2004). Major element contents alone, therefore, cannot fully reveal the processes that affected our peridotites. However, the combination of trace element concentrations (REE) and Hf-Nd isotope ratios provides key insights into the past and present melting and melt-rock interaction processes recorded by the SL peridotites, as discussed in the following.

5.1.1. The sample-specific multi-stage evolution of the peridotites

Clinopyroxenes in samples **S22–44/14** and **S22–32/1** (Figs. 3a and 4) have the highest $(Lu/Hf)_N$ (11.9 and 9.5) and $(Sm/Nd)_N$ (7.04 and 6.15) with overall LREE-depleted REE patterns, indicating that these peridotites were not geochemically modified by recent melt-rock interactions. Another sample with strong REE depletion is the peridotite **I10–63/37** that shows strongly depleted MREE and HREE, with very low Nd and Hf contents (0.020 and 0.023 times BSE) indicating high extents of melt depletion, although it shows comparatively high La, Ce, and Pr contents ($(Ce/Sm)N = 0.52$) (Figs. 3a and 4). These samples, **S22–44/14, S22–32/1, I10–63/37,** are characterized by high ε_{Hf} (47, 51, and 40, respectively) but low ε_{Nd} (−2, +10 and +3, respectively). High $^{176}Hf/^{177}Hf$ can only develop in ancient mantle residues that have preserved their high Lu/Hf for several 100–1000 Ma (Stracke et al., 2011; Sani et al., 2023). The low ε_{Nd} requires, however, that past melt-rock interaction processes have lowered their Sm/Nd preventing the evolution toward the high $^{143}Nd/^{144}Nd$ expected for ancient melt-depleted peridotites.

Alternatively, recent melt-rock reaction may have shifted the Nd isotope ratios toward those of the interacting melt while retaining relatively high Hf isotope ratios (Salters and Dick, 2002; Le Roux et al., 2007; Stracke et al., 2011; Sanfilippo et al., 2019; Tilhac et al., 2022; Sani et al., 2023; Woelki et al., 2025). The pronounced LREE-depletion of **S22–44/14** and **S22–32/1** indicates, however, that the last step of their evolution must have been renewed partial melting under the MAR without significant LREE re-enrichment by melt-rock reaction. In contrast, the relative enrichment of LREE of sample **I10–63/37** requires some degree of recent melt-rock interaction (see the high LREE-enriched patterns in red in Fig. 7b). The scenarios inferred for peridotites **S22–44/14** and **S22–32/1** are shown quantitatively in Fig. 7a and b, which illustrate the following sequence of events: ancient melting of a DM-like peridotite, accompanied by concurrent melt-rock reaction in the past (Fig. 7a), followed by recent remelting without significant melt-rock reaction (grey dotted lines Fig. 7b). Whereas the low MREE-HREE, and in particular the low Nd and Hf contents of **I10–63/37,** indicate higher extents of melt depletion than for sample **S22–44/14**, these two samples have similar ε_{Hf} - ε_{Nd} signatures. The similar isotopic signatures indicate that the two samples probably had a similar history of past melting and melt-rock reaction (Fig. 7a), but

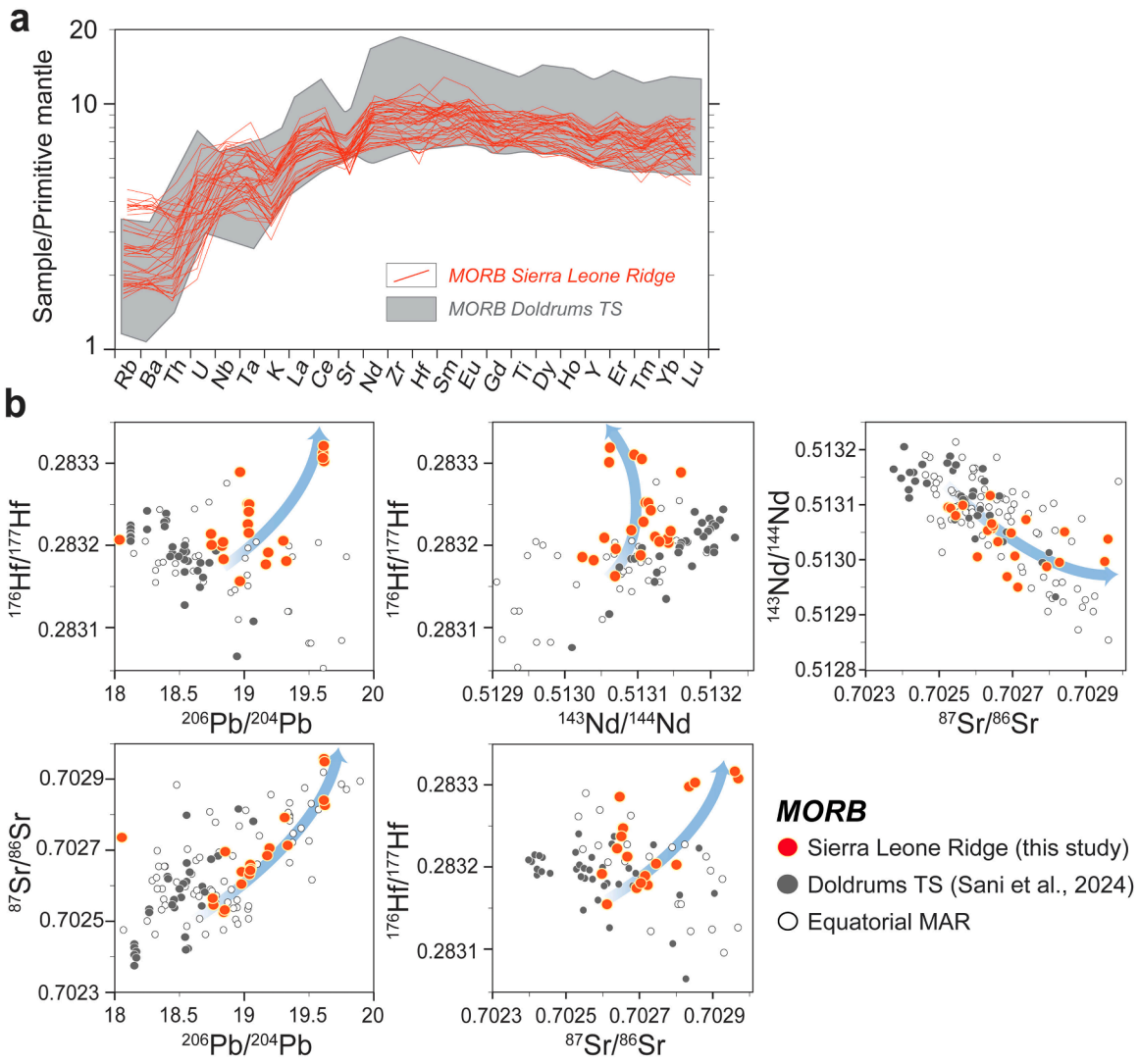

Fig. 5. Trace element compositions and Sr-Nd-Pb-Hf isotope ratios of Sierra Leone Ridge basalts. (a) Primitive mantle–normalized diagrams (McDonough and Sun, 1995) comparing the studied basalts (filled orange circles) with Doldrums TS basalts (gray shaded area) from Sani et al. (2024). All basalts are depleted in the most incompatible trace elements (e.g., LILE, LREE) relative to the less incompatible ones (e.g., HREE). On average, Sierra Leone Ridge MORB are less fractionated than those from the Doldrums transform region, which extend towards higher abundances of incompatible elements. (b) Sr, Nd, Hf, and Pb isotope ratios of basalts from the Sierra Leone Ridge, the Doldrums TS, and the regional area (PetDB, www.earthchem.org/petdb). All samples (symbols as in Fig. 2) plot within the field defined by global MORB, spanning from isotopically enriched compositions (high Sr-Pb and low Hf-Nd ratios) to more depleted ones (low Sr-Pb and high Hf-Nd ratios). However, basalts from the Sierra Leone Ridge show distinctive signatures, with elevated $^{206}Pb/^{204}Pb$, $^{87}Sr/^{86}Sr$, and $^{176}Hf/^{177}Hf$, but low $^{143}Nd/^{144}Nd$ isotopic ratios. This composition may represent a mantle component characteristic of this sector of the MAR, influenced by the widespread high Hf isotopic compositions observed in the associated mantle peridotites.

I10–63/37 melted to higher extents recently, followed by small addition of melts to account for its elevated LREE contents (Fig. 7b). We cannot exclude that this recent melt-rock reaction process was partly responsible for the low ε_{Nd}, while still preserving the original high ε_{Hf}.

Peridotites **S22–32/5, I10–5/8** and **I10–5/5** have high HREE contents (e.g. Yb_N of 2.7, 3.2 and 2.5, respectively) but low MREE contents (Fig. 3a). Because HREE are compatible elements in garnet, these peridotites must have melted little and/or melted mostly in the garnet stability field to maintain high HREE in the Cpx, even after recent remelting (Fig. 7a, green lines and dot). Sample **S22–32/5** has preserved the highest Hf and Nd isotope ratios ($\varepsilon_{Hf} = 51$ and $\varepsilon_{Nd} = 25$) of all investigated peridotites (Fig. 3a, 4a), suggesting that this peridotite has melted in the past but underwent only minimal interaction with melts, perhaps slightly decreasing the Sm/Nd so that the present-day Nd isotope ratios are slightly lower than expected for pure melting residues (Fig. 7a green line and dot). Alternatively, the higher LREE in **S22–32/5** compared to other samples (Fig. 3a) may indicate that this peridotite has reacted to a small extent with melts recently (Fig. 7b). Whether the small extent of melt-rock reaction inferred for this sample happened in the past or recently therefore remains somewhat ambiguous. The peridotites **I10–5/8** and **I10–5/5** with similar REE patterns have high ε_{Hf} of 54 and 28 but low ε_{Nd} of 11 and 12, respectively, as well as low LREE contents. Similar to samples **S22–44/14** and **S22–32/1** (Figs. 3a and 4a), the melt-rock reaction that caused the MORB-like ε_{Nd} but high ε_{Hf} values of peridotites **I10–5/8** and **I10–5/5** (Figs. 3b and 4a), must therefore have predated recent remelting.

Peridotite **I10–63–36** has Cpx with low HREE contents (i.e. $Yb_N = 1$) but flat MREE and higher MREE/LREE fractionation ($(Ce/Sm)_N = 0.09$) (Figs. 3c and 4). The low HREE contents suggest that the peridotite melted to large extent (Fig. 7a), but the high MREE/HREE indicate that it has also reacted with a melt. Melt-rock reaction could have occurred in the past, before recent melting decreased the LREE relative to MREE and HREE (Fig. 7a and b). Notably, this sample has relatively high ε_{Hf} of +31 but very low ε_{Nd} of −6 (Fig. 4). These Hf-Nd isotope signatures are most

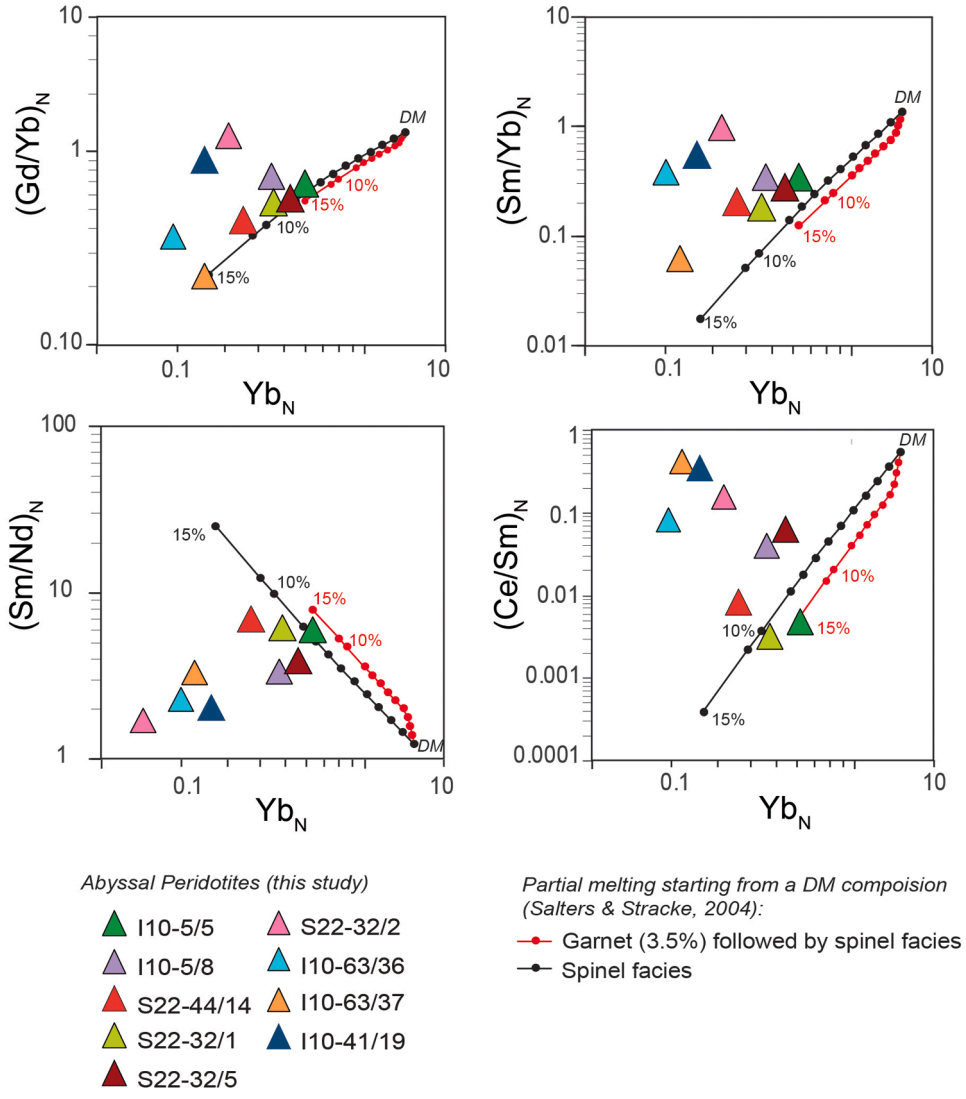

Fig. 6. Dynamic melting model. Variations of (Gd/Yb)N, (Sm/Yb)N, (Ce/Sm)N and (Sm/Nd)N versus YbN (primitive mantle normalized, Mc Donough and Sun, 1995) in cpx from Sierra Leone peridotites compared with the dynamic melting model used in Sani et al., 2020. The REE composition of a residual cpx produced by process of near-fractional melting (F = 0–14 %) starting from a DM composition from Salters and Stracke Sani et al., EPSL (2004) and using melting equations and a constant set of partition coefficients from the same study. Black lines represent melting in the spinel field, red lines 3.5 % degrees of melting in the garnet followed by further 10.5 % melting in the spinel fields. Each step represents 1 % melting. We do observe that the cpx of the studied peridotites do not follow the melting lines, suggesting that their compositions are not pure results of partial melting processes.

easily explained if the processes that have generated the isotope and geochemical composition of this peridotite happened in the following order: high extents of past melt-depletion led to very low HREE contents (Fig. 7a, possibly higher than the 7 %F represented in the figure). The flat MREE-HREE pattern, coupled to very low ε_{Nd}, is inherited from significant extents of past melt-rock reaction, while maintaining sufficiently high Lu/Hf to develop the present-day moderately high ε_{Hf} (+31). The formation of a flat REE pattern and low Nd isotope ratio requires the interaction of the mantle with incompatible element enriched melts, likely influenced by melts from an incompatible element enriched mantle component such as recycled crust (e.g., Hofmann et al., 1986; Chauvel et al., 1992; Stracke, 2012). Finally, recent remelting has decreased the LREE contents but has preserved the flat MREE-HREE pattern (Fig. 7b)

Peridotite **S22–32/2** has flat MREE-HREE pattern ($(Gd/Yb)_N$ of 1.2) and moderately fractionated LREE/MREE ratio ($(Ce/Sm)_N$ = 0.2) and thus, overall, a relatively flat REE pattern. This peridotite has ε_{Nd} of 8.5 but moderately high ε_{Hf} of 30. Hence, although some extent of melt-rock reaction is required to explain its ε_{Nd} - ε_{Hf} signatures, owing to its relatively flat REE pattern, it is inconclusive whether melt-rock reaction happened in the past or recently, or both (Fig. 7b).

Peridotite **I10–41/19** also has relatively flat MREE-HREE pattern ($(Gd/Yb)_N$ = 1) but is LREE enriched ($(Ce/Sm)_N$ = 0.4). This LREE enrichment coupled to low ε_{Hf} of 12.3 and ε_{Nd} of 1.8 suggests that recent reaction with LREE enriched melts has significantly affected the LREE contents, but also the Nd-Hf isotope ratios. To what extent this sample has also been affected by past melt-rock reaction processes is therefore difficult to infer, because the recent reaction has obscured signs of its past history of melting and melt-rock reaction (Fig. 7c).

5.1.2. *Evidence for ancient versus recent melt-rock reaction*

Remarkably, TiO_2 wt. % and HREE $(Yb)_N$ in Cpx from the peridotites of the Sierra Leone Ridge decrease with decreasing ε_{Nd} (Fig. 4b). Other incompatible major elements such as Na_2O, FeO, K_2O and Al_2O_3 wt. % do not show any correlation with Nd isotope ratios, or Yb and TiO_2 contents, and also do not correlate with Hf isotope ratios (not shown). One way to explain these observations is that the peridotites experienced high degrees of melting in the past, leading to low HREE, and,

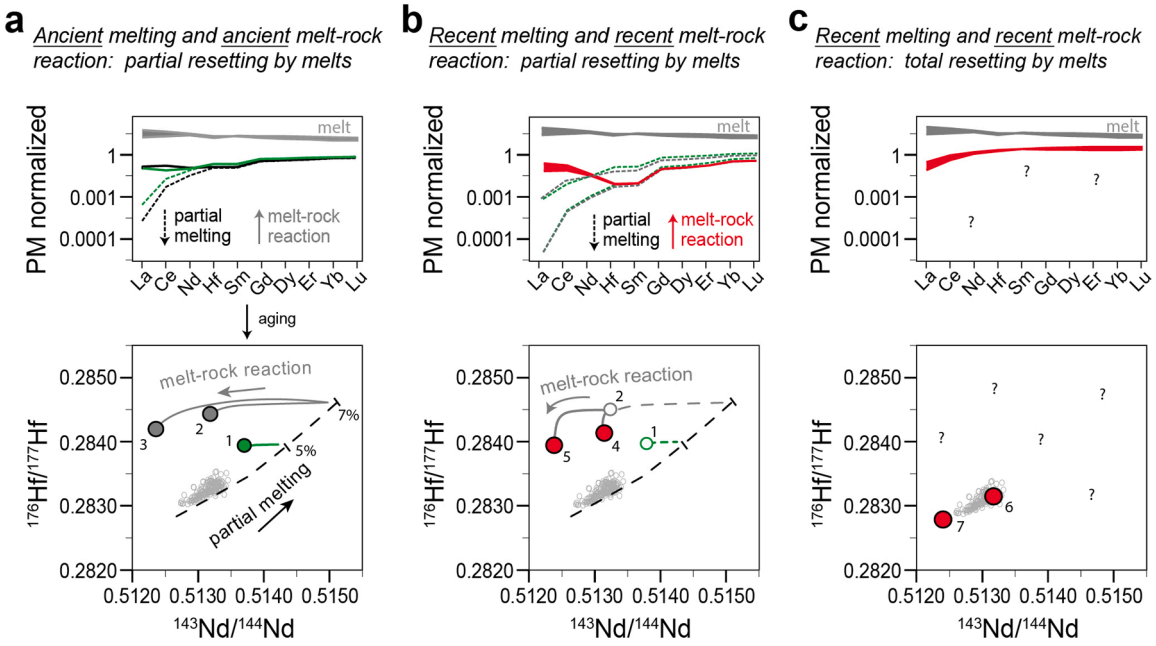

Fig. 7. Evolution of trace elements and Nd-Hf isotopes in the mantle through time as a result of melting and melt–rock reactions. The diagrams illustrate how past and recent partial melting, as well as melt–rock interactions, influence REE patterns and Nd-Hf isotope ratios of mantle peridotites. Models and calculation details follow Sani et al. (2023). Dashed lines in Nd-Hf isotopic space represent radiogenic evolution after ancient melting events, whereas solid lines depict the isotopic evolution of recent processes. Empty gray circle indicate MORB samples from the MAR (PetDB, www.earthchem.org/petdb). (a) Ancient REE depletion at 1.5 Ga (top panel) after 7 % (black dashed line) and 5 % (green dashed line) partial melting of a primitive mantle (composition from McDonough and Sun, 1995), producing the Nd-Hf isotope evolution shown by the black dashed line (bottom panel). Partial interaction of these mantle residues with isotopically distinct melts generated compositions 1 (green filled circle), 2, and 3 (gray filled circles), each with distinct Nd-Hf signatures, resulting in an isotopically heterogeneous mantle. (b) Recent melting and recent partial melt-rock reaction. Melt-modified mantle (solid green and black lines in the REE panel of (a), compositions 1 and 2, respectively) underwent further partial melting and subsequent melt–rock interaction, which altered both REE and isotopic compositions. The REE diagram (top panel) shows 3 % and 7 % partial melting (gray and green dashed lines), with melt-modified residues highlighted in red. In isotope space (bottom panel), hollow circles represent Nd–Hf isotope ratios of mantle residues after recent melting. For clarity, only residue composition 2 is shown interacting with melts, producing composition 4 (interaction with depleted MORB-like melt) and composition 5 (interaction with enriched melt). The melts involved range from N-MORB to E-MORB compositions (Gale et al., 2013). (c) Recent melting followed by complete resetting through melt interaction. Full chemical equilibration with melts erased any prior history of the peridotites, producing flat REE patterns (red lines, top panel) and Nd-Hf isotopic compositions (filled red circles, bottom panel) comparable to DM-like MORBs and isotopically enriched melts (compositions 6 and 7, respectively). Further details of the modeled compositions and results are provided in Supplementary Table S5.

more generally, incompatible element contents, thereby becoming chemically susceptible to reaction with incompatible element enriched melts. Melt-rock reaction re-enriched the LREE producing variably flat REE patterns approaching those of the melt, but had a much smaller effect on the HREE contents (note that the differences in the concentration between a MORB-like melt and variably trace element depleted peridotites are much larger for the LREE than for the HREE; Fig. 7). Recent melting decreases the LREE content, thus erasing any prior LREE enrichment, so that present-day LREE/MREE enrichments must be due to renewed melt-rock reaction. The trend defined by the HREE, TiO_2 and Nd isotope ratios shows, however, that the effects of present-day melt-rock reaction on the LREE contents are comparatively small, and thus do not introduce enough scatter to erase the correlation originating from the melt-depletion and melt-rock reaction events in the past.

5.1.3. Synthesis of peridotite evolution through time

In summary, each peridotite from the Sierra Leone Ridge has its own history of melting (at different degree) and reaction with melts, either in the past or recent, or both, involving heterogeneously melt-depleted peridotites and melts of different compositions. Nevertheless, a common feature of all the analyzed peridotites is that they record ancient melting, but also variable past melt-rock reactions that lowered their Sm/Nd more than the Lu/Hf ratios, leading to variably low ε_{Nd} (−6 to +25) but relatively high ε_{Hf} (16 – 54) today. Note that the high HREE contents that characterize most of the peridotites, which have HREE contents in cpx by far higher than a typical primitive mantle (see Fig. 3), are a robust indicator of previous melt-rock reaction events. Furthermore, the preservation of a correlation between the HREE or TiO_2 and the Nd isotope ratios reveals a limited effect of recent infiltration by melts, so that high ε_{Hf} as a sign of past melt-depletion are preserved in almost all of the abyssal peridotites studied here.

5.2. A fingerprint of an old refertilized peridotite in the erupted MORB

The MORB from the Sierra Leone (SL) Ridge are characterized by comparatively high Hf isotope ratios, in line with the composition of the peridotites from this area (Figs. 2 and 8). In Hf vs. Nd-Sr-Pb isotope plots (Fig. 5b), the SL MORB plot towards high Hf isotope ratios, but some samples diverge towards exceptionally high $^{176}Hf/^{177}Hf$, coupled with high Sr and Pb and low Nd isotope ratios (Fig. 5b). Overall, the isotopic diversity of the MORB from the SL ridge, compared to those from the MAR north of the Doldrums FZ, suggests a large contribution from melts derived from a mantle component with high Hf isotope ratios but also high Sr and Pb isotope ratios, which is distinct from the incompatible element enriched recycled crust (low Hf-Nd and high Sr-Pb isotope ratios) inferred to produce the “anomalous” MORB at 1.7°N (Figs. 2, 5, 8) (Schilling et al., 1994).

The divergence of the SL MORB toward such peculiar isotopic signatures (i.e., radiogenic Hf but low Nd and high Sr and Pb isotope ratios) shows that components with high time-integrated Lu/Hf and low Sm/Nd, but variably high Rb/Sr and U-Th/Pb contributed to formation of the local MORB. These signatures are similar to those of the analyzed peridotites, assuming that the processes that led to their low Sm/Nd also resulted in high Rb/Sr and U-Th/Pb ratios (Section 5.1). This implies

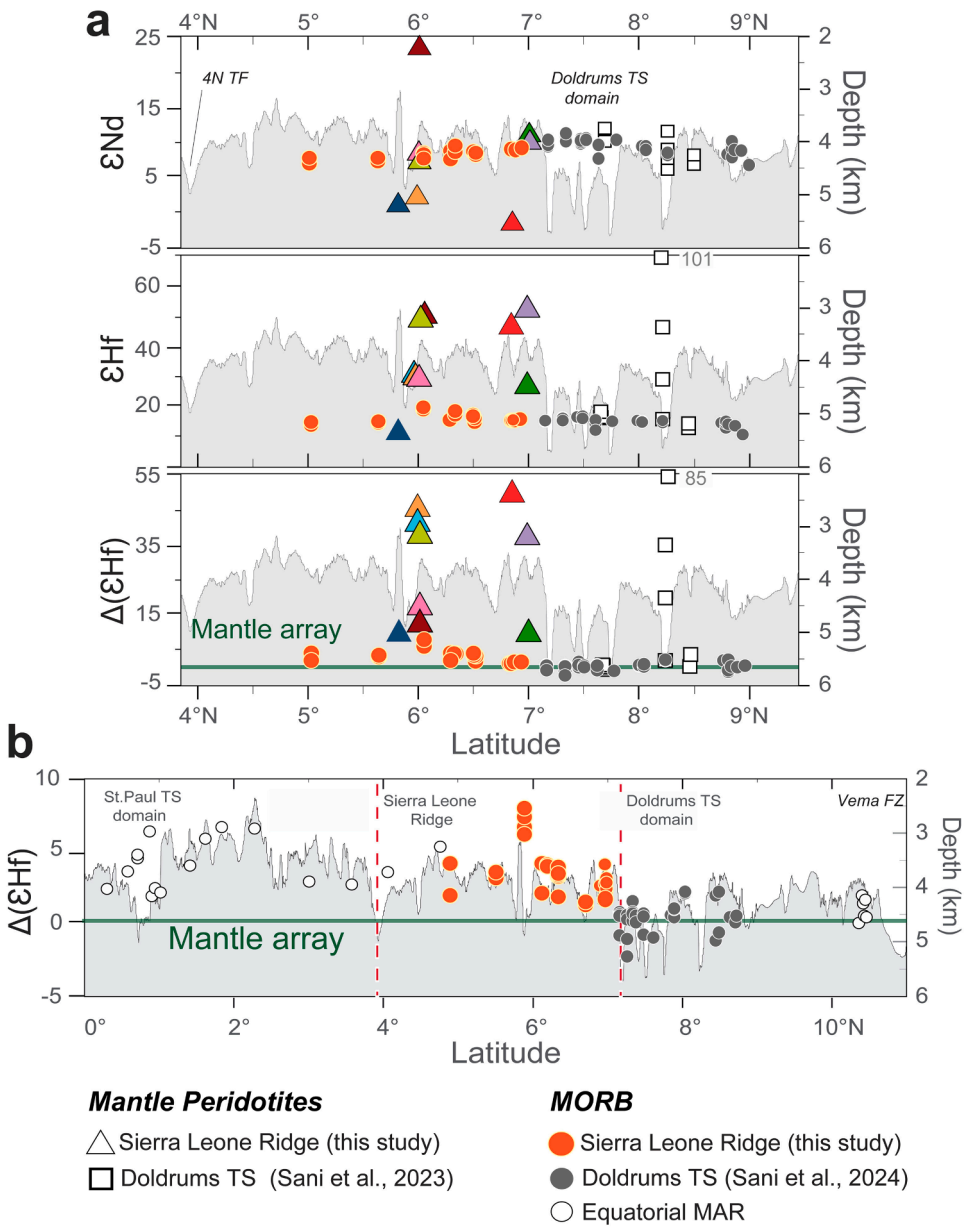

Fig. 8. Hf–Nd isotopic systematics and ΔHf variation of peridotites and associated MORBs along the Equatorial MAR. Diagrams showing ƐHf, ƐNd, and ΔHf of clinopyroxenes from peridotites and of basalts from this study, together with data from Sani et al. (2023; 2024), plotted versus latitude. (a) Basalts (symbols as in Fig. 2) and abyssal peridotites (symbols as in Fig. 4a) from the studied area and from north of the Doldrums TS. North of the Doldrums TS, sampled rocks display homogeneous ƐNd values, whereas ƐHf varies significantly but only in three peridotite samples, which shift towards higher values. South of the Doldrums TS, along the Sierra Leone Ridge, basalts show relatively homogeneous ƐNd, whereas peridotites span a wide range, from high to low values. Samples north of the Doldrums TS cluster near the mantle array, whereas samples from the Sierra Leone Ridge consistently plot above the Nd–Hf mantle array. (b) MORBs from the MAR between 0° and 11°N. These data indicate that isotopically depleted and buoyant mantle sources characterize not only the magmatism of the studied segment (4–7°N), but also the entire magmatic domain south of the Doldrums TS, even where MORBs show exceptionally high Sr and Pb isotope ratios (Schilling et al., 1994). Notably, variations in ΔHf closely follow changes in ridge-axis depth.

that melting of peridotites with similar isotopic composition as the SL peridotites contributed to the local MORB, which is in agreement with the idea that the SL peridotites experienced a prior history of partial melting and variable degrees of melt-rock reaction before they were emplaced in the Atlantic asthenosphere and remelted recently under the MAR. The association of high Hf, low Nd with high Sr and Pb isotope ratios of the SL MORB is compatible with the contribution of melts from peridotites that melted in the past (increasing Lu/Hf and, with time leading to high Hf isotope ratios), but were refertilized at the same time (decreasing Sm/Nd, but increasing Rb/Sr and U,Th/Pb, thus leading to low Nd but high Sr and Pb isotope ratios with time).

Similar to the MORB from the SL Ridge (see Fig. 2), the entire sector of the MAR between the Doldrums FZ (~ 7°N) and the St. Paul FZ (~ −1°N) plot well above the global Nd-Hf isotope trend defined by MORB and ocean island basalts (OIB), including the enriched MORB from the 1.7°N anomaly. Specifically, the variations in ΔHf (ΔHf = [ε_{Hf}-(1.55*ε_{Nd}-1.21)], Chauvel et al., 2008) of MORB along this section of the MAR differ substantially from those of the MAR segment North of the Doldrums FZ. Hence, there is a geochemical boundary corresponding to the southern transform of the Doldrums system (at 7.15°N), which divides a large-scale mantle province having basalts with comparatively high ΔHf (from 2 to 8) relative to the MORB north of Doldrums, which have ΔHf between −2 and +2, and thus lie on the global Nd-Hf isotope trend of MORB and OIB (Figs. 2 and 8). South of the Strakov FZ at 4°N no

abyssal peridotites have been sampled, but the available MORB exposed along the MAR up to −1 °N suggest the occurrence of a mantle with high Hf isotope ratios. Nevertheless, the geochemical anomaly of MORB at 1.7°N might be produced by a distinct local mantle composition.

5.3. Buoyant, refertilized mantle under the Sierra Leone Ridge

Schilling et al. (1994) inferred that MORB from the Sierra Leone (SL) Ridge are produced by melting of anomalously hot mantle, fed by the postulated SL mantle plume (Schilling et al., 1994; Skolotnev, 2014 Fig. 2). In this scenario, melting of anomalously hot mantle produces thick crust, which would explain why the SL Ridge is shallower than the MAR to the north (i.e., north of the Doldrums FZ). However, the example of high Hf isotope ratios in peridotites from the Marion Rise and the associated MORB (Woelki et al., 2025) along the Southwest Indian Ridge shows that shallow ridges do not necessarily require increased melt production due to anomalously hot mantle, but may also result from the isostatic response to passive upwelling of buoyant, melt-depleted mantle without large associated temperature variations (Zhou and Dick, 2013; Woelki et al., 2025).

Melt depletion generates light peridotites that are also strongly depleted in incompatible elements, while retaining variable amounts of Cpx (Afonso and Schutt, 2012; Stracke and Béguelin, 2024; Stracke and Salters, 2025). Such incompatible element depleted, but "fertile" (i.e., Cpx-rich) peridotites may thus still produce abundant melt (e.g., Byerly and Lassiter, 2014; Sani et al., 2020; Sanfilippo et al., 2024; Stracke and Béguelin, 2024; Stracke and Salters, 2025).

The high Hf isotope ratios observed in peridotites and associated basalts along the SL Ridge indicate that variably melt-depleted, and thus light peridotites, contributed abundant melt to the local MORB. For approximately 8 % of melting, peridotite density decreases by ~0.5 % (relative to a reference mantle density, $\rho_0 = 3300$ kg m^{-3}, Afonso and Schutt, 2012). This degree of melt-depletion makes the peridotite buoyant enough to rise without requiring a thermal contrast (a temperature increase of > 150°C would be needed to achieve a similar effect, e.g., Stracke and Beguelin, 2024). Notably, the peridotites investigated in this study were also affected, to variable extents, by melt-rock reaction. Melt-rock reaction enriches the peridotites in incompatible elements and slightly increases their Cpx contents, but these chemical and mineralogical modifications do not substantially affect their Fe content. When a harzburgite (peridotite with <5 % modal Cpx) reacts with a basaltic, incompatible element enriched melt, part of the rock is dissolved into the melt and new Cpx crystallizes. We calculated peridotite compositions and density resulting from variable extents of partial melting and melt -rock reaction using the 'Plate model' by Vernières et al. (1997), assuming partial dissolution of an harzburgitic mantle matrix (78 % ol, 20 % Opx, 2 % Cpx and initial porosity of 1 %) and simultaneous precipitation of Cpx from the reacted and modified melt with a ratio of mass assimilated to mass crystallized of ~0.99 (see model results in Sanfilippo et al., 2024). At low degrees of interaction, as suggested by the preserved high Hf isotopic composition of SL peridotites, modal Cpx contents increase by ~3 %. The density of the resulting rock, composed of 69.7 vol % olivine ($\rho = 3.2$ g/cm^3), 19.3 vol % orthopyroxene ($\rho = 3.2$ g/cm^3), 8 vol % clinopyroxene ($\rho = 3.25$ g/cm^3) and 3 vol % spinel ($\rho = 3.78$ g/cm^3), increases by ~0.0019 g/cm^3, which corresponds to a 0.05 % density increase. This resulting density increase is about ten times lower than the ~ 0.5 % density reduction by ca. 8 % partial melting (see above). Hence, the addition of small aliquots of melt to a melt-depleted peridotite does not substantially increase its density, although the refertilized rock has higher modal cpx content and is enriched in incompatible elements. Indeed, melt productivity of peridotite is nearly constant as long as Cpx is present (Walter and Cottrell, 2025), so that an ancient refertilized peridotite similar to the one produced by our plate model has enough modal cpx (~ 8 vol %) to produce substantial amount of melt during recent melting event. An ancient melt-depleted peridotite that was refertilized by a basaltic melt concurrent to ancient melting remains unusually light and thus compositionally buoyant, but is also chemically fertile. After several 100 Ma to Ga residence in the convecting mantle, such a buoyant refertilized peridotite can remelt under present-day mid-ocean ridges or ocean islands (e.g. Sanfilippo et al., 2024; Béguelin et al., 2025) and contribute significant amounts of melt to the local basalts.

5.4. Influence of a hot plume at the Sierra Leone Ridge?

The bathymetry in Fig. 1a shows that the ridge between the St. Paul and Doldrums FZs is shallower (from 4500 m up to 2500 m depth) than the ridge north of the Doldrums FZ (from 5500 m up to 4000 m depth). The change in depth of the ridge axis could be explained by a southward increase in mantle potential temperature along the ridge segment between 0 and 10°N, as consequence of the emplacement of hot material from the Sierra Leone plume (Schilling et al., 1994). However, here we show that the geochemical characteristics of the peridotites and basalts exposed along the Sierra Leone ridge suggest that the elevated ridge topography (Fig. 1) is likely due to the upwelling of material that consists mainly of depleted, buoyant peridotites. The high melt-production of this sector of MAR could also explain the lack of large lithospheric discontinuities along the ridge axis between 0 and 7°N, where the morphology of the ridge is continuous. Indeed, north of the Doldrums FZ, the ridge is not only deeper but also laterally displaced by several long-offset transform faults.

We therefore suggest that the high melt production that formed the off axis Ceará and Sierra Leone Rises (Fig. 1) is not caused by an impinging plume, i.e., the alleged "Sierra Leone Mantle plume" (Schilling et al., 1994). Rather, intermittent upwelling of a heterogeneous bulge of material, mostly composed of highly depleted, light peridotite, since ~80 Ma has locally increased mantle buoyancy, thus mantle flux per unit time through the sub-ridge melting region. Indeed, those parts of the upwelling mantle that contain, on average, more melt-depleted peridotite have different buoyancy, and in an isothermal mantle, intermittently increase the upwelling velocity. This may occur without associate temperature variations in a hot plume as suggested for Iceland and Hawaii (Sanfilippo et al., 2024; Béguelin et al., 2025), but can also occur in colder mantle that rises passively under mid-ocean ridges (see quantitative discussion in Béguelin et al., 2025). Hence, a burst of light, depleted mantle through the sub-ridge melting region could have led to the formation of an on-axis magmatic plateau for ca. 30 Ma, now preserved as the Sierra Leon Rise to the east and Ceará Rise to the west of the present Mid-Atlantic Ridge.

6. Conclusions

This study combines geochemical and isotopic data from basalts and abyssal peridotites to reveal a complex history of the mantle under the Sierra Leone (SL) Ridge.

The Hf-Nd isotope ratios and chemical composition of the studied peridotites reflect a combination of several factors: the degree of past and recent melt-depletion, and reaction with trapped or migrating melts of variable composition. A distinct correlation between HREE content and Nd isotope ratios in clinopyroxene suggests that peridotites with the highest degree of ancient depletion experienced the most extensive interaction with enriched melts in the past (Fig. 4b). Preserving this correlation also implies recent melt-rock reactions subsequent to recent remelting under the SL Ridge were limited.

The widespread high Hf isotope ratios in both abyssal peridotites and MORB from the same area (Fig. 8) suggest that peridotites similar to the investigated SL peridotites are the dominant component of the local mantle and, hence, influence the isotopic composition of the basalts from the Sierra Leone Rise. Because the chemical and isotopic composition of the SL peridotites shows that they have melted extensively before recent upwelling under the SL Ridge, they are compositionally light. Their excess buoyancy may therefore increase the rate of

upwelling, and thus the amount of melt production per time under the MAR. This effect may explain the elevated topography and abundant magmatism that characterizes this portion of the MAR (0–7°N), and be responsible for the formation of the Sierra Leone and Ceará Rise plateaus ~80 Ma ago (Schilling et al., 1994). Intrinsic density variations of the passively upwelling, sub-ridge mantle may therefore cause intermittent periods of excess of melt production, and thus thicker-than-normal oceanic crust, at the SL ridge or elsewhere along the global Mid-Ocean ridge system. The associated compositional heterogeneity of the heterogeneous peridotites and minor recycled crust may also influence the chemical and isotopic composition of the generated basalts (e.g., Stracke and Béguelin, 2024). However, neither the elevated topography (with or without thick oceanic crust), nor the spatially and temporally variable chemical and isotopic composition of MORB necessitates the "interaction" of mid-ocean ridges with actively upwelling, hot mantle plumes.

CRediT authorship contribution statement

Camilla Sani: Writing – review & editing, Writing – original draft, Methodology, Investigation, Conceptualization. **Alessio Sanfilippo:** Writing – review & editing, Supervision, Methodology, Funding acquisition, Conceptualization. **Felix Genske:** Methodology, Investigation. **Carlotta Ferrando:** Writing – review & editing, Methodology. **Daniele Brunelli:** Resources, Methodology. **Anna Cipriani:** Resources. **Alexander Peyve:** Resources, Funding acquisition. **Sergey Skolotnev:** Resources, Funding acquisition. **Marco Ligi:** Resources, Funding acquisition, Conceptualization. **Andreas Stracke:** Writing – review & editing, Methodology, Funding acquisition, Conceptualization.

Declaration of competing interest

The authors declare that they have no known competing financial interests or personal relationships that could have appeared to influence the work reported in this paper.

Acknowledgements

This study was supported by the German Research Foundation by research Grant STR853/14–1 and STR853/15–1 to A.St. Also was supported by Accordo Bilaterale CNR/RFBR 2018–2020 (project no CUP-B36C17000250005) and by the Italian Programma di Rilevante Interesse Nazionale (project nos. PRIN_2017KY5ZX8 to M.L. and PRIN_2022PC9NME to A. Sanfilippo) and by the Russian Foundation for the Basic Research (project no 18–55–7806 Ital_t to S. Skolotnev), Russian Foundation for the Basic Research (project no FMMG-2022–0003 to A. Peyve).

Supplementary materials

Supplementary material associated with this article can be found, in the online version, at doi:10.1016/j.epsl.2025.119812.

Data availability

All data are available in the supplementary material.

References

Afonso, J.C., Schutt, D.L., 2012. The effects of polybaric partial melting on density and seismic velocities of mantle restites. Lithos 134, 289–303.
Béguelin, P., Stracke, A., Ballmer, M.D., Huang, S., Willig, M., Bizimis, M., 2025. Variations in Hawaiian plume flux controlled by ancient mantle depletion. AGU Adv. 6 (2), e2024AV001434. https://doi.org/10.1029/2024AV001434.
Basile, C., Girault, I., Paquette, J.L., Agranier, A., Loncke, L., Heuret, A., Poetisi, E., 2020. The jurassic magmatism of the Demerara Plateau (offshore French Guiana) as a remnant of the Sierra Leone hotspot during the Atlantic rifting. Sci. Rep. 10 (1), 7486.
Blichert-Toft, J., Albar`ede, F., 1997. The Lu-Hf isotope geochemistry of chondrites and the evolution of the mantle-crust system. Earth Planet. Sci. Lett. 148 (1–2), 243–258.
Bonatti, E., Seyler, M., Sushevskaya, N., 1993. A cold suboceanic mantle belt at the Earth's equator. Science 261 (5119), 315–320.
Bonatti, E., Ligi, M., Gasperini, L., Peyve, A., Raznitsin, Y., Chen, Y.J., 1994. Transform migration and vertical tectonics at the Romanche fracture zone, equatorial Atlantic. J. Geophys. Res. 99 (B11), 21779–21802.
Brunelli, D., Seyler, M., 2010. Asthenospheric percolation of alkaline melts beneath the St. Paul region (Central Atlantic Ocean). Earth Planet. Sci. Lett 289 (3–4), 393–405. https://doi.org/10.1016/j.epsl.2009.11.028.
Brunelli, D., Seyler, M., Cipriani, A., Ottolini, L., Bonatti, E., 2006. Discontinuous melt extraction and weak refertilization of mantle peridotites at the Vema lithospheric section (Mid-Atlantic Ridge). J. Petrol. 47 (4), 745–771.
Byerly, B.L., Lassiter, J.C., 2014. Isotopically ultradepleted domains in the convecting upper mantle: implications for MORB petrogenesis. Geology 42 (3), 203–206.
Chauvel, C., Hofmann, A.W., Vidal, P., 1992. HIMU-EM: the French Polynesian connection. Earth Planet. Sci. Lett. 110 (1–4), 99–119.
Chauvel, C., Lewin, E., Carpentier, M., Arndt, N.T., Marini, J.C., 2008. Role of recycled oceanic basalt and sediment in generating the Hf–Nd mantle array. Nat. Geosci. 1 (1), 64–67.
Dick, H.J., Bullen, T., 1984. Chromian spinel as a petrogenetic indicator in abyssal and alpine-type peridotites and spatially associated lavas. Contrib. Miner. Pet. 86, 54–76.
Ferrando, C., Borghini, G., Sani, C., Genske, F., Ligi, M., Stracke, A., Sanfilippo, A., 2024. Deep segregation and crystallization of ultra-depleted melts in the sub-ridge mantle. Chem. Geol. 644, 121840.
Gale, A., Dalton, C.A., Langmuir, C.H., Su, Y., Schilling, J.-G., 2013. The mean composition of ocean ridge basalts. Geochem. Geophys. Geosyst. 14, 489–518.
Godard, M., Bodinier, J.-L., Vasseur, G., 1995. Effects ofmineralogical reactions on trace element redistributions in mantle rocks during percolation processes: a chromatographic approach. Earth Planet. Sci. Lett. 133, 449–461. https://doi.org/10.1016/0012-821X(95)00104-K.
Guarnieri, L., Nakamura, E., Piccardo, G.B., Sakaguchi, C., Shimizu, N., Vannucci, R., Zanetti, A., 2012. Petrology, trace element and Sr, Nd, Hf isotope geochemistry of the North Lanzo peridotite massif (Western Alps, Italy). J. Petrol. 53, 2259–2306. https://doi.org/10.1093/petrology/egs049.
Hellebrand, E., Snow, J.E., 2003. Deep melting and sodic metasomatism underneath the highly oblique-spreading Lena Trough (Arctic Ocean). Earth Planet. Sci. Lett. 216 (3), 283–299.
Hofmann, A.W., Jochum, K.P., Seufert, M., White, W.M., 1986. Nb and Pb in oceanic basalts: new constraints on mantle evolution. Earth Planet. Sci. Lett. 79 (1–2), 33–45.
Jochum, K.P., Weis, U., Stoll, B., Kuzmin, D., Yang, Q., Raczek, I., Jacob, D.E., Stracke, A., Birbaum, K., Frick, D.A., Günther, D., 2011. Determination of reference values for NIST SRM 610–617 glasses following ISO guidelines. Geostand. Geoanal. Res. 35, 397–429.
Kelley, K.A., Kingsley, R.H., Schilling, J.-G., 2013. Composition of plume-influenced mid-ocean ridge lavas and glasses from the Mid-Atlantic Ridge, East Pacific Rise. Galápagos Spreading Cent. Gulf Aden Geochem. Geophys. Geosyst. 14, 223–242. https://doi.org/10.1002/ggge.20049.
Klein, E.M., Langmuir, C.H., 1987. Global correlations of ocean ridge basalt chemistry with axial depth and crustal thickness. J. Geophys. Res. Solid Earth 92, 8089–8115.
Le Roux, V., Bodinier, J.L., Tommasi, A., Alard, O., Dautria, J.M., Vauchez, A., Riches, A. J.V., 2007. The Lherz spinel lherzolite: refertilized rather than pristine mantle. Earth Planet. Sci. Lett. 259 (3–4), 599–612. https://doi.org/10.1016/j.epsl.2007.05.026.
Le Voyer, M., Cottrell, E., Kelley, K.A., Brounce, M., Hauri, E.H., 2015. The effect of primary versus secondary processes on the volatile content of MORB glasses: an example from the equatorial Mid-Atlantic Ridge (5 N–3 S). J. Geophys. Res.: Solid Earth 120 (1), 125–144.
Ligi, M., Bortoluzzi, G., 1989. PLOTMAP: geophysical and geological applications of good standard quality cartographic software. Comput. Geosci. 15, 519–585.
Ligi, M., Bonatti, E., Gasperini, L., Poliakov, A.N.B., 2002. Oceanic broad multifault transform plate boundaries. Geology 30, 11–14.
Ligi, M., Cuffaro, M., Muccini, F., Bonatti, E., 2022. Generation and evolution of the oceanic lithosphere in the North Atlantic. Riv. Nuovo Cimento. 45, 587–659.
Long, X., Van der Zwan, F.M., Geldmacher, J., Hoernle, K., Hauff, F., Garbe-Schönberg, C.D., Augustin, N., 2020. Insights into the petrogenesis of an intraplate volcanic province: sr-Nd-Pb-Hf isotope geochemistry of the Bathymetrists Seamount Province, eastern equatorial Atlantic. Chem. Geol. 544, 119599.
Lugmair, G.W., Galer, S.J.G., 1992. Age and isotopic relationships among the angrites Lewis Cliff 86010 and Angra dos Reis. Geochim. Cosmochim. Acta 56 (4), 1673–1694.
Münker, C., Weyer, S., Scherer, E., Mezger, K., 2001. Separation of high field strength elements (Nb, Ta, Zr, Hf): and Lu from rock samples for MC-ICPMS measurements. Geochem. Geophys. Geosyst. 2 (G3).
McDonough, W.F., Sun, S.S., 1995. The composition of the Earth. Chem. Geol. 120 (3–4), 223–253.
Morrow, T.A., Mittelstaedt, E.L., 2021. Quantifying periodic variations in hotspot melt production. J. Geophys. Res.: Solid Earth 126 (7), e2021JB021726.
Niu, Y., 2004. Bulk-rock major and trace element compositions of abyssal peridotites: implications for mantle melting, melt extraction and post-melting processes beneath mid-ocean ridges. J. Pet. 45, 2423–2458.
Peyve, A.A., Savel'eva, G.N., Skolotnev, S.G., Simonov, V.A., 2003. Tectonics and origin of the oceanic crust in the region of "dry" spreading in the Central Atlantic (7°10′-5° N). Geotectonics. 37 (2), 75–94.
Salters, V.J.M., Dick, H.J.B., 2002. Mineralogy of the mid-ocean-ridge basalt source from neodymium isotopic composition of abyssal peridotites. Nature 418, 68–72.

Salters, V.J.M., Stracke, A., 2004. Composition of the depleted mantle. Geochem. Geophys. Geosyst. 5, Q05004.
Sanfilippo, A., Salters, V., Tribuzio, R., Zanetti, A., 2019. Role of ancient, ultra-depleted mantle in Mid-Ocean-Ridge magmatism. Earth Planet Sci. Lett. 511, 89–98. https://doi.org/10.1016/j.epsl.2019.01.018.
Sanfilippo, A., Stracke, A., Genske, F., Scarani, S., Cuffaro, M., Basch, V., Borghini, G., Brunelli, D., Ferrando, C., Peyve, A.A., Ligi, M., 2024. Upwelling of melt-depleted mantle under Iceland. Nat. Geosci. 17 (10), 1046–1052.
Sani, C., Sanfilippo, A., Ferrando, C., Peyve, A.A., Skolotonev, S.G., Muccini, F., Zanetti, A., Basch, V., Palmiotto, C., Bonatti, E., Ligi, M., 2020. Ultra-depleted melt refertilization of mantle peridotites in a large intra-transform domain (Doldrums Fracture Zone; 7–8◦ N, Mid Atlantic Ridge). Lithos 374, 105698.
Sani, C., Sanfilippo, A., Peyve, A.A., Genske, F., Stracke, A., 2023. Earth mantle's isotopic record of progressive chemical depletion. AGU Adv 4 (2), e2022AV000792.
Sani, C., Sanfilippo, A., Skolotnev, S., Ligi, M., Genske, F., Stracke, A., 2024. Sampling Earth's mantle at intra-transform spreading ridges. Geochim. Cosmochim. Acta 374, 156–172.
Savel'eva, G.N., Bortnikov, N.S., Peyve, A.A., Skolotnev, S.G., 2006. Ultramafic rocks from the Markov deep in the Rift Valley of the Mid-Atlantic Ridge. Geochem. Int. 44 (11), 1105–1120. https://doi.org/10.1134/S0016702906110024.
Schilling, J.G., Hanan, B.B., McCully, B., Kingsley, R.H., Fontignie, D., 1994. Influence of the Sierra Leone mantle plume on the equatorial Mid-Atlantic Ridge: a Nd-Sr-Pb isotopic study. J. Geophys. Res.: Solid Earth 99 (B6), 12005–12028.
Schutt, D.L., Lesher, C.E., 2006. Effects of melt depletion on the density and seismic velocity of garnet and spinel lherzolite. J. Geophys. Res.: Solid Earth 111 (B5).
Seyler, M., Lorand, J.P., Toplis, M.J., Godard, G., 2004. Asthenospheric metasomatism beneath the mid-ocean ridge: evidence from depleted abyssal peridotites. Geology 32 (4), 301–304.
Seyler, M., Lorand, J.-P., Dick, H.J.B., Drouin, M., 2007. Pervasive melt percolation reactions in ultra-depleted refractory harzburgites at the Mid-Atlantic Ridge, 15° -20°N: ODP hole 1274A. Contrib. Mineral. Petrol. 153 (3), 303–319. https://doi.org/10.1007/s00410-006-0148-6.
Skolotnev, S., Peyve, A.A., Lyapunov, S.M., Simonov, V.A., Glazyrin, Yu.E., Yu. Kolobov, V., 2003. MAR volcanism in the Sierra Leone Fracture Zone region, Central Atlantic. Russ. J. Earth Sci. 5 (2), 101–123.
Skolotnev, S.G., Sanfilippo, A., Peyve, A.A., Muccini, F., Sokolov, Y.S., Sani, C., Dobroliubova, K.O., Ferrando, C., Chamov, N.P., Palmiotto, C., Pertsev, A.N., Bonatti, E., Cuffaro, M., Gryaznova, A.C., Sholukhov, K.N., Bich, A.S., Ligi, M., 2020. Large-scale structure of the Doldrums multi-fault transform system (7–8◦N Equatorial Atlantic): results from the 45th Expedition of the R/V A. N. Strakhov. Ofioliti. 45, 25–41.
Skolotnev, S.G., 2014. New isotopic data for Mid-Atlantic Ridge basalts from the Arkhangelsk-Sierra Leone fracture zone (central Atlantic). Dokl. Earth Sci. 459 (1), 1429–1435.
Sleep, N.H., 2002. Ridge-crossing mantle plumes and gaps in tracks. Geochem. Geophys. Geosystems. 3 (12), 1–33.
Stracke, A., Béguelin, P., 2024. Basalts record a limited extent of mantle depletion: cause and chemical geodynamic implications. Geochem. Perspect. Lett. 32, 21–26.
Stracke, A., Salters, V.J., 2025. The role of peridotite for oceanic volcanism. Geochem. Geophys. Geosystems 26 (8), e2025GC012463.
Stracke, A., Snow, J.E., Hellebrand, E., von der Handt, A., Bourdon, B., Birbaum, K., Günther, D., 2011. Abyssal peridotite Hf isotopes identify extreme mantle depletion. Earth Planet. Sci. Lett. 308, 359–368. https://doi.org/10.1016/j.epsl.2011.06.012.
Stracke, A., 2012. Earth's heterogeneous mantle: a product of convection-driven interaction between crust and mantle. Chem. Geol. 330-331, 274–299. https://doi.org/10.1016/j.chemgeo.2012.08.007.
Stracke, A., 2021. A process-oriented approach to mantle geochemistry. Chem. Geol. 579, 120350. https://doi.org/10.1016/j.chemgeo.2021.120350.
Tilhac, R., Begg, G.C., O'Reilly, S.Y., Griffin, W.L., 2022. A global review of Hf-Nd isotopes: new perspectives on the chickenand- egg problem of ancient mantle signatures. Chem. Geol. 609, 121039.
Todd, E., Stracke, A., Scherer, E.E., 2015. Effects of simple acid leaching of crushed and powdered geological materials on high-precision Pb isotope analyses. Geochem. Geophys. Geosyst. 16 (7), 2276–2302.
Udintsev, G.B., 1996). Equatorial segment of the Mid-Atlantic Ridge. Technical Series. Intergov. Oceanogr. Comm. Sér. Tech., 46. UNESCO: Paris, pp. 122.
Vernières, J., Godard, M., Bodinier, J.L., 1997. A plate model for the simulation of trace element fractionation during partialmelting and magma transport in the Earth's upper mantle. J. Geophys. Res. Solid Earth 102, 24771–24784.
Walter, M., Cottrell, E., 2025. Equilibrium constraints on partial melting in the upper mantle. In: Treatise in Geochemistry, 3rd ed. ed, pp. 231–273.
Warren, J.M., Shimizu, N., Sakaguchi, C., Dick, H.J.B., Nakamura, E., 2009. An assessment of upper mantle heterogeneity based on abyssal peridotite isotopic compositions. J. Geophys. Res. 114, B12203. https://doi.org/10.1029/2008JB006186.
Willig, M., Stracke, A., Beier, C., Salters, V.J., 2020. Constraints on mantle evolution from Ce-Nd-Hf isotope systematics. Geochim. Cosmochim. Acta 272, 36–53. https://doi.org/10.1016/j.gca.2019.12.029.
Woelki, D., Salters, V., Stracke, A., Genske, F., White, G., Brunelli, D., 2025. Abundant ancient melt depleted peridotite beneath the Marion Rise, Southwest Indian Ocean, effects on basalt composition and dynamic topography. Geochem. Geophys. Geosystems 26 (9), e2025GC012418.
Zhou, H., Dick, H.J., 2013. Thin crust as evidence for depleted mantle supporting the Marion Rise. Nature 494 (7436), 195–200.